Optics Letters

Nonlinear optical memory effect

A. Fleming,[1] C. Conti,[2] T. Vettenburg,[3] and A. Di Falco[1,*]

[1]School of Physics and Astronomy, University of St. Andrews, North Haugh, St. Andrews KY16 9SS, UK
[2]Institute for Complex Systems, National Research Council (ISC-CNR), Via dei Taurini 19, 00185 Rome, Italy
[3]School of Science and Engineering, University of Dundee, Nethergate, Dundee, DD1 4HN, UK
*Corresponding author: adf10@st-andrews.ac.uk

Received 6 August 2019; revised 31 August 2019; accepted 2 September 2019; posted 3 September 2019 (Doc. ID 374858); published 25 September 2019

Light propagating through random media produces characteristic speckle patterns, directly related to the large multitude of scattering events. These complex dynamics remarkably display robustness to perturbation of the incoming light parameters, maintaining correlation in the scattered wavefront. This behavior is known as the optical memory effect. Here we unveil the properties of the nonlinear optical memory effect, which occurs when an optothermal nonlinearity perturbs the random material. The effect is characterized through a series of pump and probe experiments in silica aerogel, in the visible range. This additional degree of freedom further generalizes the memory effect, opening the road to applications based on the nonlinear response of random media.

https://doi.org/10.1364/OL.44.004841

Scattering media are often seen as a hindrance to information transfer by light propagation. With the advent of the transmission matrix formalism, there is now a deeper understanding of the deterministic nature of light scattering. This allows scattering media to be turned into polarimeters [1], spectrometers [2], and lenses that focus in space [3] and time [4]. However, making a full measurement of a materials transmission or scattering matrix, comprising many millions of elements [5], is not always practical, particularly for media that change over time, or where access to the target plane is not readily available, such as in biological samples. Despite the complex and highly specific nature of the measurement, there exist significant correlations in the speckle patterns produced by scattering media when the incoming wavefront undergoes slight perturbations in position and angle. These short-range (C1 type) correlations [6] are known as the optical memory effect [7]. These correlations have already demonstrated their importance in biomedical imaging techniques [8], the ultrafast dephasing of light through nonlinear perturbation [9], and the measurement of transport properties through effect refractive index variation in random media [10]. The range of such correlations is enhanced in media that are either thin [11] or that are thick and scatter predominantly in the forward direction [12]—which is the case for much of biological media.

There are two forms to this effect, which are known as the "tilt–tilt" and "shift–shift" memory effects. In the former, a tilt to the incoming wavefront will result in a tilt of the scattered wavefront, registering as a shift in any distribution of scattered intensity on the image plane [6,11]. The latter effect is a Fourier twin of the first effect in which a shift of the incoming wavefront will result in a shift of the scattered wavefront [12]. Shortly after this, Osnabrugge *et al.* showed that these two effects could be combined, extending the range the effect would maintain correlation in the scattering state. This combination is known as the generalized optical memory effect [7].

The optical memory effect builds upon increasing experimental understanding of deterministic light scattering, from initial iterative experiments in wavefront shaping that turn opaque media into powerful lenses, to optical transmission matrices. In general, control over deterministic light scattering is more complete with the more degrees of freedom that are manipulated.

One such further degree of freedom is nonlinear properties. In addition to acting as a degree of freedom, nonlinear and scattering environments often occur in tandem. Consideration of these nonlinear effects is, therefore, an important extension to the range of applications using the earlier mentioned techniques. Such potential applications include nonlinear imaging [13,14] and laser microsurgery [15]. There are also applications where high-power beams cause optothermal-based nonlinearities in biological media [16,17,18,19].

Mirroring developments in the manipulation of light scattering in linear media, wavefront shaping in nonlinear media has also become a useful tool as an additional degree of control. For example, a focus point produced through wavefront shaping can be partially eliminated, or restored, through optical pumping. Recently, we have shown that it is possible to encode the nonlinearity of a specific material through nonlinear transmission matrices [20].

Here, as a natural extension to light scattering control, mirroring the development in linear scattering systems, we present another form to the optical memory effect. We term this the "nonlinear optical memory effect" (NL-OMEM). We manipulate the scattering media itself, through the use of the large optothermal nonlinearity of silica aerogel [21].

The power in this effect comes from the additional degrees of freedom present in these systems compared to the ballistic transport of light. An additional degree of freedom that is now being investigated in order to manipulate light to a greater extent is nonlinearity. Here, we present another form to the

optical memory effect, where instead of manipulating the wavefront, we manipulate the scattering media itself, through the use of the large optothermal nonlinearity of silica aerogel [21]. We term this the "nonlinear optical memory effect" (NL-OMEM).

For the experimental measurements of the NL-OMEM, a vital requirement of the scattering medium in addition to the existence of nonlinear behavior is the ability to generate highly localized perturbations as to manipulate only the required multiple scattering light paths of the medium to illicit a NL-OMEM response. Silica aerogel is an ultraporous material made of sparse silica aggregates, which exhibits an extremely low thermal conductivity, even lower than that of air, due to the Knudsen effect [22]. Thanks to this property, aerogel localizes heat very effectively [23], which in turn mediates optothermal nonlinearities at powers that are low compared to what would be usually expected of nonlinear processes, on the order of 10^{-12} m^2/W. This unique combination of properties leads to aerogel being used in a large variety of optical and thermal applications such as shockwaves [23], microfluidics [24], plasmonics [25], and where lightweight insulation is required [22].

We adopt a standard base catalyzed silica precursor approach for the fabrication of aerogel used for this work. We mixed tetramethyl orthosilicate (TMOS), methanol, and ammonium hydroxide (aq) in a 2:4:1 ratio, for a total volume of 1 mL. The TMOS and ammonium hydroxide were purchased from Sigma Aldrich. The ammonium hydroxide was diluted to 35 μL per 100 mL of ultrapure water also from Sigma Aldrich. The stock chemicals of methanol and acetone were purchased from Fischer Scientific. This mixture was poured into an acrylic (PMMA), producing a cube-shaped gel with a volume of 1 cm^3. After approximately 1 h, the sol gelated. Following gelation, a series of acetone baths, each lasting 24 h, washed the solgels, dissolving the PMMA cuvette and removing residual chemical impurities leftover from the gelation process. We produced the aerogel by supercritically drying the solgel using a custom-made CO_2 critical point drier, which took 12 h.

For the determination of the NL-OMEM, we employ the use of a pump–probe optical setup, shown in Fig. 1.

Figure 1 shows the optical system used for the measurement of the NL-OMEM. The probe beam is a $\lambda_{probe} = 532$ nm, MLL-III-532-400mW diode laser from Changchen New Industries Optoelectronics Technology Co. Ltd. We coupled this laser to multimode fiber, the emission of which was collimated by a lens. This coupling gave an output power of approximately 100 mW. A half-wave plate adjusted the polarization of the probe for the optimal phase-only operation of the spatial light modulator (SLM). Polarizers ensure we imaged only scattered photons.

The SLM, an HSP512 from Meadowlark, then modulates the phase front of the light. Using this, we perform wavefront shaping [26] through a custom-built genetic algorithm program [27], to generate two laterally separated focus points. Each area of focus was a 5 × 5 pixel region of interest (ROI) on the CCD camera.

This pair of focus points allows us to identify both shifts and distortions in the scattered wavefront, through the relative intensity, position, and separation of the focus points. With the genetic algorithm approach, we found an approximately 80-fold enhancement with respect to the background intensity.

Focusing through random media is enabled by the control of the dephasing between the multiple light scattering paths in

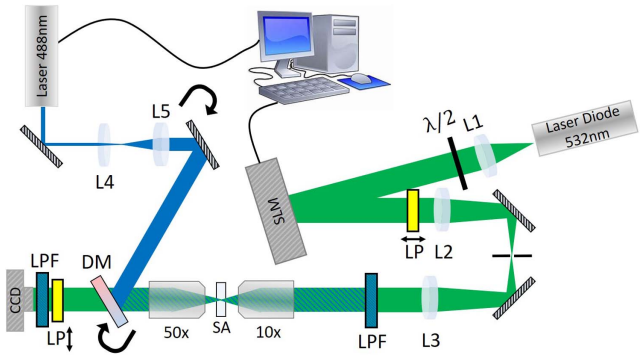

Fig. 1. Optical setup used for manipulation of the measurement of the NL-OMEM. The probe is sub-mW 532 nm CW source. This probe is collimated to overfill an SLM, which patterns the wavefront that then passes through a 4-f system, selecting the first order. A 10 × objective focuses the beam within the aerogel, which is then collected by a 50× objective. The pump was a Toptica i-BeamSmart 200 mW 488 nm CW laser, expanded and collimated to fill the back focal lens of the 50× objective. The scattered transmission was recorded continuously by a Basler 1920ac CCD camera. LPF, long-pass filters at 500 nm cutoff are used to block the pump beam from key pieces of apparatus and prevent diffusely scattered light from reaching the camera. DM, a 505 nm long-pass dichroic mirror. LP, linear polarizers, with polarization axis noted by a black arrow. Curved arrow, represent optics that are on adjustable mounts.

the medium [28]. This extends to nonlinear media also [29,30]. Through pump–probe experiments, it is possible to eliminate this focusing through nonlinear dephasing, either electronically [31], or optothermally (reference us). For the latter, we have recently shown that it is possible to measure the transmission matrix [32,33] of the perturbed system (reference us) allowing for a predictive response to nonlinear effects in scattering systems. Here we aim to employ these nonlinear perturbations, the NL-OMEM, while still maintaining correlation in the scattered wavefront. Thermal effects due to pumping result in an expansion of the silica matrix, lowering its density and resulting in a refractive index change, which dephases and can guide light leading to a displacement of intensity at the output plane [34].

We perturb the material using the pump beam, not at the location of the focus but rather over a range of distances between 0.47 mm and 0.78 mm, at powers between 50 mW and 150 mW. Use of higher powers resulted in permanent deformation of the SA. This layout is described in Fig. 2. This pumping causes a localized expansion to one side of the ROI, causing a shift in the spots but also a dephasing impacting the peak intensity. The diminishing in the correlation of the scattered wavefront with a shift is common to all memory effect types. Figure 3 shows an example of this perturbation.

To act as a reference to the NL-OMEM, we compare it to the shift–shift memory effect. In our genetic algorithm process, the species to be assessed are displayed on the SLM with the addition of a phase-blazed grating, in order to select the first order of reflected light. By adjusting the frequency of this additional grating, a tilt in the wavefront is produced, which manifests itself as a shift in the sample between the microscope objectives.

We correlate images to measure the performance of both the memory effects using MATLAB's `xcorr2` function on the

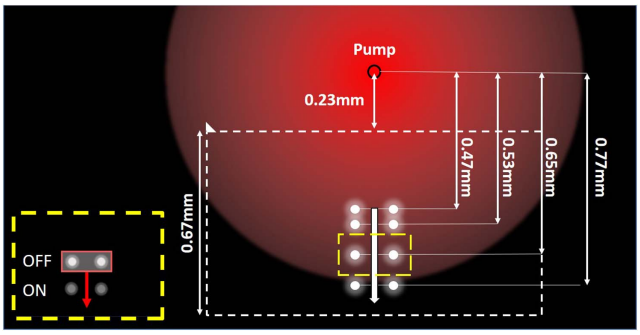

Fig. 2. Schematic showing the geometry of the pump–probe experiments. The white box indicates the imaging area. The large red diffuse spot represents the thermal radial profile. Each of the four pairs of white points indicates different positions at which the output is optimized. Using pairs of focus points, it is possible to identify both shifts and distortions in the scattered wavefront, through both the relative intensity, position, and separation of the focus points. The yellow inset shows the effect of the pump on an individual pair of focus points. The direction of shift in the focus points is indicated by the red arrow, along with a representation of that shift. To evaluate the effect of the perturbation, a ROI around the spots in their initial state (OFF), represented by the white shaded region, is correlated with the surrounding area of the scattered state during pumping (ON).

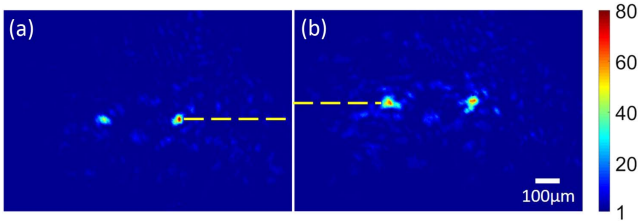

Fig. 3. Example of the NL-OMEM through nonlinear perturbation. Using a pump power of 150 mW at a distance of 0.53 mm from the pump. Left, original wavefront. Right, perturbed wavefront exhibiting the NL-OMEM.

raw image data. The inset of Fig. 2 illustrates how this performed in general for both the shift–shift and the NL-OMEM. Cross-correlation measurements are made as the blaze grating is stepped, or each frame of recording during the pumping for the NL-OMEM.

Figure 4 shows the results of these cross-correlation measurements for a range of pump powers and pump-ROI separations. Each line represents the position of the maximum of the correlations over time, as the aerogel heats up because of the pumping. The maximum shift for each curve is obtained when the dynamics reach a steady state. At a pump-ROI separation of 0.78 mm, the NL-OMEM effect is comparable to the shift–shift memory effect. All powers follow the same linear change in correlation with the system's initial state; however, the extent is less than that of the shift–shift memory effect. For Figs. 4(b)–4(d), with closer pump-ROI separations, the dynamics are more complex.

First, there exists a linear relationship between power and the end point of the correlation curve (indicated by thin black line). This relationship is the result of a reduction in the final

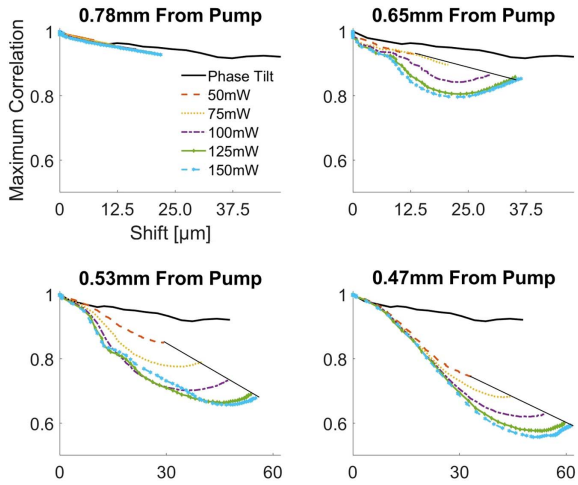

Fig. 4. Correlation of the area surrounding the ROI with respect to its shift by memory effects. The colored lines refer to changes in correlation due to NL-OMEM. The thick black line refers to changes in correlation due to the shift–shift memory effect. (a) The pump beam acting 1250 pixels/0.78 mm vertically displaced from the ROI. (b) 1050 pixels/0.65 mm. (c) 850 pixels/0.53 mm. (d) 750 pixels/0.47 mm. In every case, the system was pumped for 1 min. The thin black line highlights the linear trend in the final correlation of the perturbed system with pump power.

intensity of these spots relative to the background intensity. We can understand the reduction in intensity as a nonlinear dephasing of the system, or the addition of new nonlinear multiple light scattering paths, which are out of phase with the optimized spots. We demonstrated this principle in our recent work understanding this on the measurement of nonlinear transmission matrices, where linear dephasing with power was also evident [20].

Second, there is a nonlinearity to the correlation that in some cases, particularly at the higher pump powers, results in a degree of recovery towards the end of the pump when the thermal effect saturates. We understand this from a thermal standpoint. Upon switching on the pump, the aerogel begins to heat in the pump's immediate vicinity. This process initially generates a very steep and rapidly increasing temperature gradient. This steep gradient is an additional source of perturbation, which acts to distort further the shape of the optimized spots. However, as the aerogel approaches thermal equilibrium, this additional gradient, which exists on top of the one that is left upon reaching equilibrium, dissipates. As such, the additional distortion on the optimized ROIs diminishes, and a small recovery in correlation occurs.

The memory effect in random media can be used as a way to maintain the correlation of wavefronts while they are perturbed. This effect can, therefore, be used for beam steering and imaging purposes, where reoptimizing wavefronts or making a transmission matrix measurement is not practical. These memory effects, known as the "tilt–tilt" and "shift–shift" memory effects, can be combined to extend their range. With our result, we extend the applicability of the memory effect paradigm to nonlinear samples with all-optical control of the material properties, for known pumping conditions. Additionally, for our specific case, there exists a pumping regime where the degradation of the memory effect with increasing perturbation is similar to that of the linear memory effects. Since the NL-OMEM is independent of the

level of correlation, it has the potential to extend further the range of memory effects, beyond that achievable with the generalized memory effect, where the rate of degradation in the linear memory effects becomes too high. A further possibility is to use a temporally varying and spatially structured pump illumination, to create dynamic nonlinear landscapes for an optimized and iterative approach to the generation of memory effects.

In conclusion, we have demonstrated the existence of a new form of optical memory effect, which is present in nonlinear systems. This effect grants us an additional degree of freedom in the control of light scattering systems, allowing for the generation of even more powerful optical devices based on random media.

Funding. Engineering and Physical Sciences Research Council (EPSRC) (EP/M508214/1); European Research Council (ERC) (819346); QuantERA ERA-NET (731473).

Acknowledgment. A. D. F. and A. F. thank EPSRC. C. C. acknowledges QuantERA ERA-NET (Project QUOMPLEX). A. D. F. is supported by the ERC. The research data underpinning this publication can be accessed at https://doi.org/10.17630/f6966b28-a467-4d3a-af7a-2a79bccb3757.

Disclosures. The authors declare no conflicts of interest.

REFERENCES

1. T. W. Kohlgraf-Owens and A. Dogariu, Opt. Lett. **35**, 2236 (2010).
2. B. Redding, S. F. Liew, R. Sarma, and H. Cao, Nat. Photonics **7**, 746 (2013).
3. E. Van Putten, D. Akbulut, J. Bertolotti, W. L. Vos, A. Lagendijk, and A. Mosk, Phys. Rev. Lett. **106**, 193905 (2011).
4. T. Chaigne, O. Katz, A. C. Boccara, M. Fink, E. Bossy, and S. Gigan, Nat. Photonics **8**, 58 (2014).
5. A. P. Mosk, A. Lagendijk, G. Lerosey, and M. Fink, Nat. Photonics **6**, 283 (2012).
6. S. Feng, C. Kane, P. A. Lee, and A. D. Stone, Phys. Rev. Lett. **61**, 834 (1988).
7. G. Osnabrugge, R. Horstmeyer, I. N. Papadopoulos, B. Judkewitz, and I. M. Vellekoop, Optica **4**, 886 (2017).
8. S. Schott, J. Bertolotti, J.-F. Léger, L. Bourdieu, and S. Gigan, Opt. Express **23**, 13505 (2015).
9. M. Abb, E. P. Bakkers, and O. L. Muskens, Phys. Rev. Lett. **106**, 143902 (2011).
10. S. Faez, P. Johnson, and A. Lagendijk, Phys. Rev. Lett. **103**, 053903 (2009).
11. I. Freund, M. Rosenbluh, and S. Feng, Phys. Rev. Lett. **61**, 2328 (1988).
12. B. Judkewitz, R. Horstmeyer, I. M. Vellekoop, I. N. Papadopoulos, and C. Yang, Nat. Phys. **11**, 684 (2015).
13. D. Yelin and Y. Silberberg, Opt. Express **5**, 169 (1999).
14. B. G. Saar, C. W. Freudiger, J. Reichman, C. M. Stanley, G. R. Holtom, and X. S. Xie, Science **330**, 1368 (2010).
15. C. L. Hoy, O. Ferhanoglu, M. Yildirim, K. H. Kim, S. S. Karajanagi, K. M. C. Chan, J. B. Kobler, S. M. Zeitels, and A. Ben-Yakar, IEEE J. Sel. Top. Quantum Electron. **20**, 242 (2014).
16. M. Motamedi, A. J. Welch, W.-F. Cheong, S. A. Ghaffari, and O. Tan, IEEE J. Quantum Electron. **24**, 693 (1988).
17. W.-C. Lin, M. Motamedi, and A. J. Welch, Appl. Opt. **35**, 3413 (1996).
18. C. W. Connor and K. Hynynen, Phys. Med. Biol. **47**, 1911 (2002).
19. M. Ith, M. Frenz, and H. P. Weber, Appl. Opt. **40**, 2216 (2001).
20. A. Fleming, C. Conti, and A. Di Falco, Ann. Phys. **531**, 1900091 (2019).
21. M. C. Braidotti, S. Gentilini, A. Fleming, M. C. Samuels, A. Di Falco, and C. Conti, Appl. Phys. Lett. **109**, 041104 (2016).
22. M. A. Aegerter, N. Leventis, and M. M. Koebel, *Aerogels Handbook* (Springer, 2011).
23. S. Gentilini, F. Ghajeri, N. Ghofraniha, A. Di Falco, and C. Conti, Opt. Express **22**, 1667 (2014).
24. L. Xiao and T. A. Birks, Opt. Lett. **36**, 3275 (2011).
25. M. D. Grogan, M. D. Rollings, L. Xiao, W. J. Wadsworth, R. England, S. Maier, and T. A. Birks, in *Quantum Electronics and Laser Science Conference* (Optical Society of America, 2010), paper JThE21.
26. I. M. Vellekoop, Opt. Express **23**, 12189 (2015).
27. D. B. Conkey, A. N. Brown, A. M. Caravaca-Aguirre, and R. Piestun, Opt. Express **20**, 4840 (2012).
28. I. M. Vellekoop and A. Mosk, Opt. Lett. **32**, 2309 (2007).
29. O. Katz, E. Small, Y. Guan, and Y. Silberberg, Optica **1**, 170 (2014).
30. H. Frostig, E. Small, S. Derevyanko, and Y. Silberberg, "Focusing coherent light through a nonlinear scattering medium," arXiv:1607.08105 (2016).
31. T. Strudley, R. Bruck, B. Mills, and O. L. Muskens, Light Sci. Appl. **3**, e207 (2014).
32. S. Popoff, G. Lerosey, R. Carminati, M. Fink, A. Boccara, and S. Gigan, Phys. Rev. Lett. **104**, 100601 (2010).
33. S. Popoff, G. Lerosey, M. Fink, A. C. Boccara, and S. Gigan, New J. Phys. **13**, 123021 (2011).
34. O. Korotkova, Opt. Lett. **40**, 284 (2015).